

# Coherent Excitation-Selective Spectroscopy of Multipole Resonances

Xu Fang,<sup>1,\*</sup> Ming Lun Tseng,<sup>2</sup> Din Ping Tsai,<sup>2,3</sup> and Nikolay I. Zheludev<sup>1,4,†</sup>

<sup>1</sup>*Optoelectronics Research Centre and Centre for Photonic Metamaterials,  
University of Southampton, Southampton SO17 1BJ, United Kingdom*

<sup>2</sup>*Department of Physics, National Taiwan University, Taipei 10617, Taiwan*

<sup>3</sup>*Research Center for Applied Sciences, Academia Sinica, Taipei 115, Taiwan*

<sup>4</sup>*Centre for Disruptive Photonic Technologies, Nanyang Technological University,  
Singapore 637371, Singapore*

(Received 16 August 2015; revised manuscript received 6 October 2015; published 27 January 2016)

Thin films of functional materials, from graphene to semiconductor heterostructures, and from nanomembranes to Langmuir-Blodgett films play key roles in modern technologies. For such films optical interrogation is the main and often the only practical method of characterization. Here, we show that characterization of the optical response of thin films can be greatly improved with a type of coherent spectroscopy using two counterpropagating beams of light. The spectroscopy is selective to particular types of multipole resonances that form the absorption spectrum of the film, and therefore can reveal lines that are hidden in conventional absorption spectroscopy. We explicitly demonstrate selectivity of this spectroscopy in a series of proof-of-principle experiments with plasmonic metamaterial arrays designed to exhibit different multipole resonances. We further demonstrate the analytic potential of this spectroscopy by extracting the hidden resonance from the spectrum of a complex nanostructure.

DOI: 10.1103/PhysRevApplied.5.014010

## I. INTRODUCTION

The study of multipole excitations in matter is a key theme in photonics research that has become even more important in nanosystems [1–14]. In this paper, we propose and report a spectroscopic technique to detect multipole resonances in matter with increased selectivity. Recently, it was shown that the strength of absorption in a thin film depends on the position of the film in a standing wave [15,16]. The spectroscopic technique proposed in this work goes much further: it exploits the fact that by placing a subwavelength thin film at the magnetic field node (where the magnetic field and electric field gradient vanish) or the electric field node (where the electric field vanishes) in a standing wave, one can selectively emphasize electric dipole or magnetic dipole and electric quadrupole resonances, correspondingly [see Fig. 1(a)]. Such selectivity gives the opportunity to detect resonances hidden by strong lines. Here, we illustrate this in a series of proof-of-principle experiments by selectively detecting multipole resonances and by demonstrating the detection of a hidden absorption line in a complex spectrum.

Indeed, the excitation-selective nature of the coherent spectroscopy can be understood by considering the Hamiltonian  $H_{\text{int}}$  of the interaction between electromagnetic radiation and matter [18]:

$$H_{\text{int}} = \frac{1}{c} \hat{\mathbf{d}} \frac{\partial \mathbf{A}}{\partial t} - \frac{1}{c} \left( \frac{d\hat{\mathbf{q}}^{il}}{dt} - e_{ilj} \hat{\mathbf{m}}^j \right) \nabla_l \mathbf{A}_i, \quad (1)$$

where  $\mathbf{A}$  is the vector potential of the electromagnetic field,  $\hat{\mathbf{d}}$ ,  $\hat{\mathbf{q}}$ ,  $\hat{\mathbf{m}}$  are the operators of electric dipole, electric quadrupole, and magnetic dipole moments of the medium, respectively,  $c$  is the speed of light,  $t$  is the time, and  $e_{ilj}$  is the Levi-Civita symbol with  $i$ ,  $l$ , and  $j$  denoting a permutation of the Cartesian coordinates  $x$ ,  $y$ , and  $z$ . For a standing wave formed by two coherent linearly polarized waves counterpropagating in  $\pm z$  directions and oscillating at frequency  $\omega$ ,  $\mathbf{A}_x = A_0 \cos(\omega t - kz) + A_0 \cos(\omega t + kz)$ , where  $A_0$  is the amplitude of the vector potential and  $k$  is the wave vector. The Hamiltonian now is reduced to

$$H_{\text{int}} = 2A_0 \frac{1}{c} \left[ \left( \frac{d\hat{\mathbf{q}}^{xz}}{dt} + \hat{\mathbf{m}}^y \right) k \cos(\omega t) \sin(kz) - \hat{\mathbf{d}}^x \omega \sin(\omega t) \cos(kz) \right]. \quad (2)$$

For a subwavelength thin film located at the electric node ( $E$  node) of the standing wave, where  $\cos(kz) = 0$ , the electric dipole interaction vanishes while magnetic dipole and electric quadrupole interactions become the dominant terms of the Hamiltonian. On the contrary, for the same sample located at the magnetic node ( $B$  node), where  $\sin(kz) = 0$ , magnetic dipole and electric quadrupole interactions vanish while the electric dipole interaction becomes the dominant term. This analysis implies that

\*To whom all correspondence should be addressed.  
x.fang@soton.ac.uk

†To whom all correspondence should be addressed.  
niz@orc.soton.ac.uk

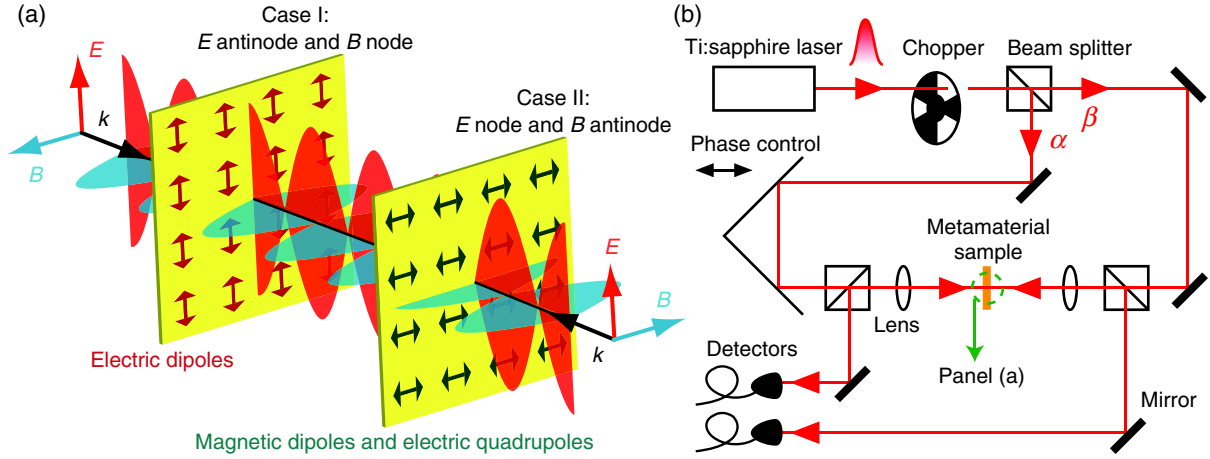


FIG. 1. Selective excitation of coherent spectroscopy for ultrathin films: principle and experimental setup. (a) In a standing wave formed by two counterpropagating normal incident laser beams, the absorption of a subwavelength thin film depends on its position. At the electric antinode and magnetic node (case I), the electric dipole absorption is at its maximum, while the magnetic dipole and electric quadrupole absorption vanishes. On the contrary, at the electric node and magnetic antinode (case II), the electric dipole resonance is suppressed and the magnetic dipole and electric quadrupole resonances are selectively excited. (b) Schematic illustration of the coherent excitation spectrometer (see the Supplemental Material [17] for details) with an enlarged view around the sample shown in (a).

coherent absorption can be measured for any film of subwavelength thickness and no requirement exists on the level of the sample's reflection or transmission.

As one can see from the derivation above [Eqs. (1) and (2)], the technique can separate the electric dipole from the magnetic dipole in absorption. It can also separate the electric dipole from the electric quadrupole. However, it cannot separate the magnetic dipole from the electric quadrupole since they simultaneously reach zero at the  $B$  node. Here, we shall note that the interference of multiple waves can, in principle, create any value of magnitude and gradient of magnetic and electric fields at a given point in free space [19]. Therefore, we argue that more elaborate versions of our technique using multiple beam interference could be better suited for distinguishing contributions of higher-order multipoles.

A spectrometer based on a Mach-Zehnder interferometer arrangement is utilized for experimental demonstration [see Fig. 1(b)]. A femtosecond laser is used as the light source for its widely tunable wavelength (from 700 to 1040 nm). A standing wave is generated from two loosely focused counterpropagating laser beams,  $\alpha$  and  $\beta$ , at the sample position. By adjusting the phase difference between the two beams, the metamaterial position is swept through field nodes and antinodes, and the output light intensity is recorded simultaneously. By repeating this process at different wavelengths, two absorption spectra lines are generated, with one induced by electric dipole resonance and the other magnetic dipole and electric quadrupole resonances. Assisted with numerical calculation, we are able to assign absorption peaks to different resonances (see the Supplemental Material [17] for more details).

## II. COHERENT CONTROL OF ELECTRIC DIPOLE RESONANCE

The first metamaterial sample in this work is a planar array of slit nanoantennas [see Figs. 2(a) and 2(b)] made from a  $\text{MgF}_2/\text{Au}/\text{Si}_3\text{N}_4$  thin film [20]. Its optical response is dominated by an electric dipole resonance [21–24], as the metasurface does not support other multipoles when illuminated at normal incidence [25,26]. Figures 2(c) and 2(d) show the experimental and numerically simulated absorption spectra [27–29] at the electric field antinode ( $E$  antinode) and the node ( $E$  node) of a standing wave, together with those in a traveling wave (the  $\text{MgF}_2$  side is illuminated), where experimental spectra show good agreement with the theoretical simulation. The peak wavelength of the traveling-wave absorption coincides with that at the  $E$  antinode. At the  $E$  antinode, the experimental and theoretically simulated absorption at around 870 nm are 0.89 and 0.99, respectively; both of them are close to total absorption. These absorption values are almost doubled from the traveling-wave absorption. In comparison, the absorption at the  $E$  node is much smaller, with the experimental and theoretical absorption at 0.07 and 0.01, respectively, at around 870 nm. The experimental value is slightly higher than the simulation, which is attributed to experimental imperfections.

Figure 2(e) shows induced surface charges at the  $E$  antinode, where charges with an opposite sign at an opposite wall resemble the electric dipole resonance [21–24]. The amplitude of the induced charges in this case is much larger than that excited by a traveling wave [see Fig. 2(f)]. This indicates a stronger electric dipole resonance of the metamaterial at the  $E$  antinode. Very different from that in Figs. 2(e) and 2(f), Fig. 2(g) shows no

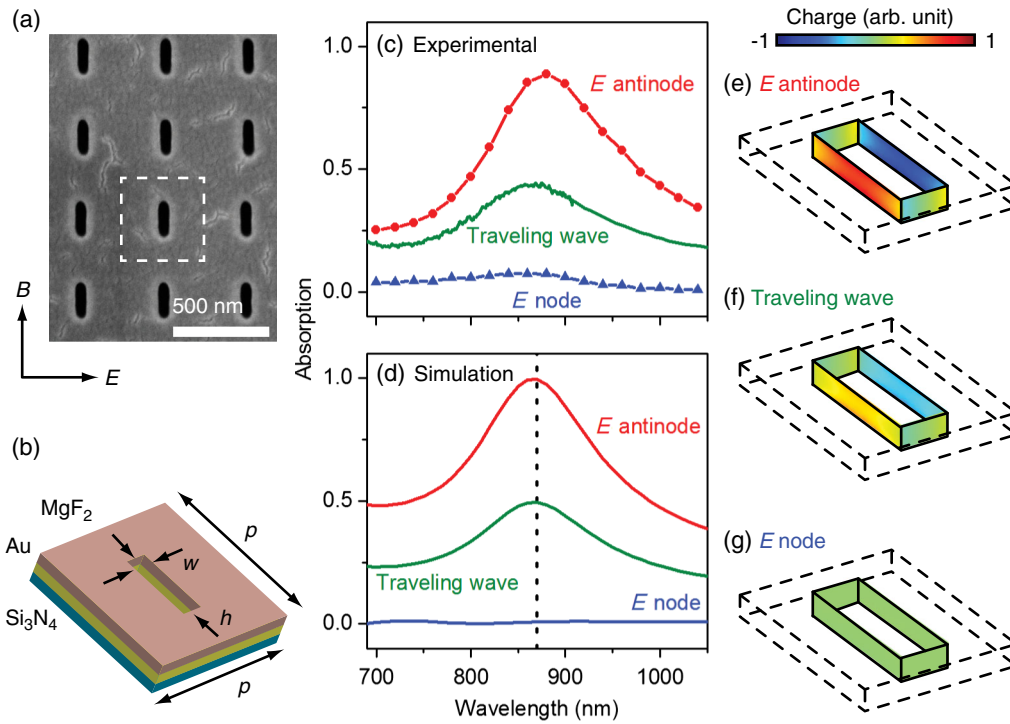


FIG. 2. Coherent control of electric dipole resonance in metamaterial. (a) SEM image of the slit nanoantenna metamaterial. Unit cell of the metamolecule is marked with the white dashed line. The polarization of the incident light is depicted. (b) Dimensions of a unit cell:  $p = 430$  nm,  $h = 180$  nm, and  $w = 60$  nm. (c),(d) Experimental and numerically simulated absorption spectra of the slit nanoantennas at the  $E$  antinode (red line) and the  $E$  node (blue line) of a standing wave, and in a traveling wave (green line). (e)–(g) Corresponding surface charge-density distribution on the inner walls of the slit in the Au layer. The wavelength is 870 nm [highlighted by the dashed line in (d)]. All panels are shown at the same color scale.

discernible charge accumulation at the  $E$  node. Both the spectra and the charge distribution clearly demonstrate that the electric dipole resonance of the slit nanoantennas can be significantly amplified or suppressed by selecting the excitation mode of the coherent spectroscopy.

### III. COHERENT CONTROL OF THE MAGNETIC DIPOLE AND ELECTRIC QUADRUPOLE

The second sample is a multilayered nanowire metamaterial [see Figs. 3(a) and 3(b)] for which the optical response is dominated by magnetic dipole and electric quadrupole resonances [30–34]. Figures 3(c) and 3(d) show the experimental and simulated absorption spectra at the magnetic field antinode ( $B$  antinode), the magnetic field node ( $B$  node), and in a traveling wave. Because of their asymmetric shape, the nanowires show different absorption spectra with the changing illumination direction (see Fig. S1 in the Supplemental Material [17]) and the average is shown here. The experimental absorption spectra have good agreement with the theoretical simulation [see Figs. 3(c) and 3(d)]: The absorption at the  $B$  antinode is considerably stronger than that in the traveling wave, and they show similar resonance features; meanwhile, the absorption is suppressed at the  $B$  node. The resonance is broader and weaker in the experiment than in the simulation, which may come from imperfections such as the thickness fluctuation of the  $\text{Si}_3\text{N}_4$  layer. The absorption at the  $B$  node comes from the electric dipole contribution.

Figure 3(e) shows the antiparallel electric displacement current in the Au layers and a strong magnetic field inside

the  $\text{Si}_3\text{N}_4$  layer at the  $B$  antinode. Both of them are the characteristics of magnetic dipole and electric quadrupole resonances of the metamaterial. The strength of the central magnetic hot spot is much bigger than the traveling-wave case [see Fig. 3(f), the top surface is illuminated]. In comparison, at the  $B$  node [see Fig. 3(g)], the induced electric displacement current is observed only in the top Au layer, and the magnetic hot spot is significantly suppressed. The results in Fig. 3 clearly demonstrate that, the same as the electric dipole resonance, the magnetic dipole and electric quadrupole resonances can also be actively controlled by the coherent spectroscopy technique.

### IV. RECOVERY OF THE HIDDEN RESONANCE AND THE MANIPULATION OF HOT SPOTS

A multilayered asymmetric split ring slit metamaterial, the third metamaterial sample, is designed for the demonstration of the recovery of a hidden resonance in the coherent spectroscopy. The SEM image and schematic illustration of the sample are shown in Figs. 4(a) and 4(b), respectively. The experimental and theoretically simulated absorption spectra of the sample under the three excitation conditions are shown in Figs. 4(c) and 4(d), respectively. In comparison with the traveling wave spectra, the  $E$ -antinode spectra exhibit a similar Fano-type profile [35–37] but have greater absorption. As discussed above, this result indicates that the Fano-type resonance of the complex metamaterial is induced by the electric field of incident light. For both the  $E$ -antinode and the traveling-wave spectra, measured absorption

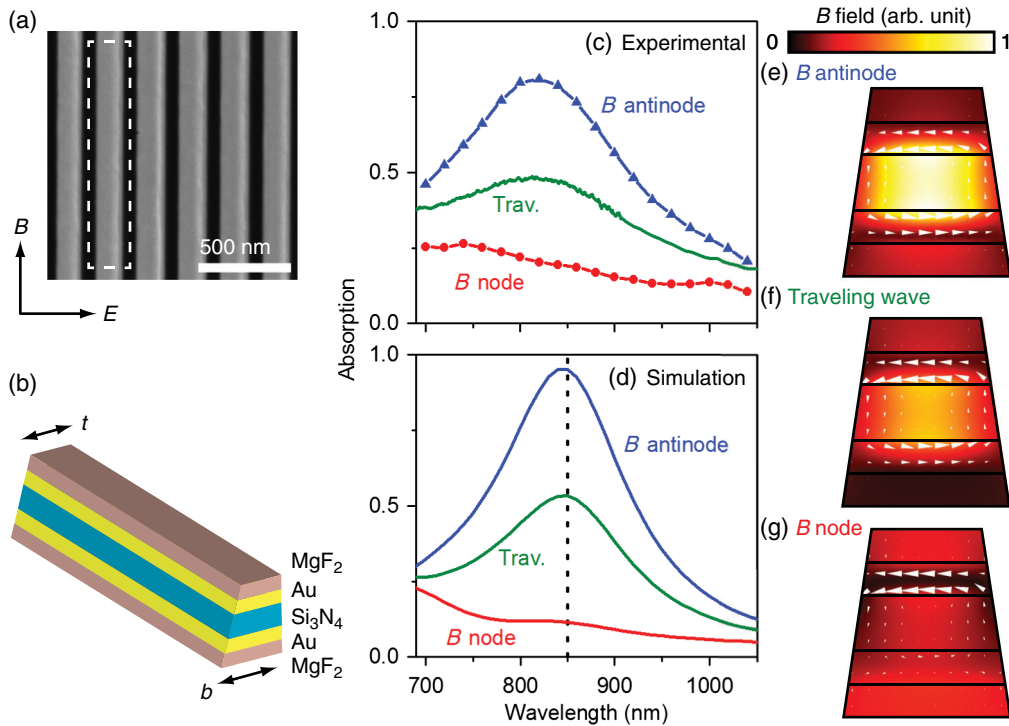


FIG. 3. Coherent control of magnetic dipole and electric quadrupole resonances in metamaterial. (a) SEM image of the nanowire metamaterial. Polarization of the incident light is depicted. Unit cell of the metamolecule is marked with the white dashed line. (b) Dimension of a unit cell,  $t = 100$  nm and  $b = 150$  nm. The periodicity is 220 nm and the wire length is  $30 \mu\text{m}$ . (c),(d) Experimental and simulated absorption spectra of the nanowires at the  $B$  antinode (blue line), the  $B$  node (red line), and in a traveling wave (green line). (e)–(g) Corresponding magnetic field (color map) and induced displacement current (white arrows) at the cross section of the metamolecule at the resonance wavelength [850 nm, highlighted in (d)].

peaks are slightly weaker and shifted in wavelength compared to the simulation. This may be attributed to experimental imperfections such as the inhomogeneity of the nanostructure.

Most interestingly, the  $E$ -node spectra in both the experiment and simulation [see Figs. 4(c) and 4(d)] are dominated by a single resonance feature at around 910 nm. Based on the discussion above, we conclude that this

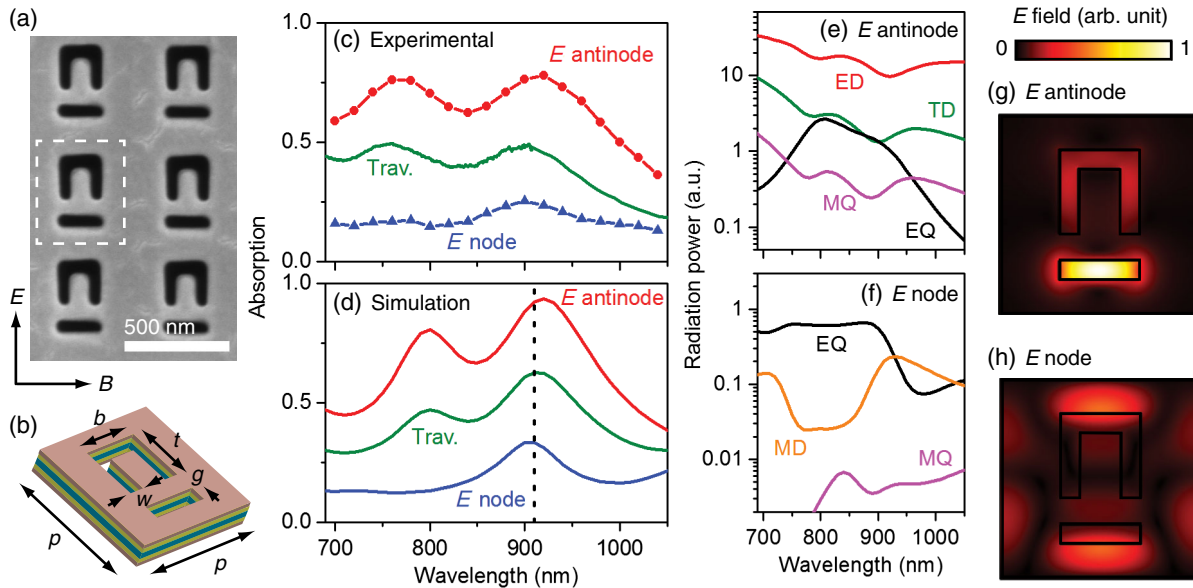


FIG. 4. Recovery of the hidden resonance and manipulation of near-field hot spots in the metamaterial. (a) SEM image of the multilayered asymmetric ring slit metamaterial. The polarization of the incident light is depicted. The unit cell of the metamolecule is marked with the white dashed line. (b) Dimensions of a unit cell:  $p = 520$  nm,  $b = 210$  nm,  $t = 220$  nm,  $g = 70$  nm, and  $w = 50$  nm. (c),(d) Experimental and simulated absorption spectra of the sample at the  $E$  antinode (red line), at the  $E$  node (blue line), and in the traveling wave (green line). (e)–(f) Leading terms of multipole radiation power at (e) the  $E$  antinode and (f) the  $E$  node. ED, electric dipole; MD, magnetic dipole; TD, toroidal dipole; EQ, electric quadrupole; and MQ, magnetic quadrupole. (g),(h) Electric field in the middle of the  $\text{Si}_3\text{N}_4$  layer at the resonance wavelength of the hidden peak [910 nm, highlighted in (d)].

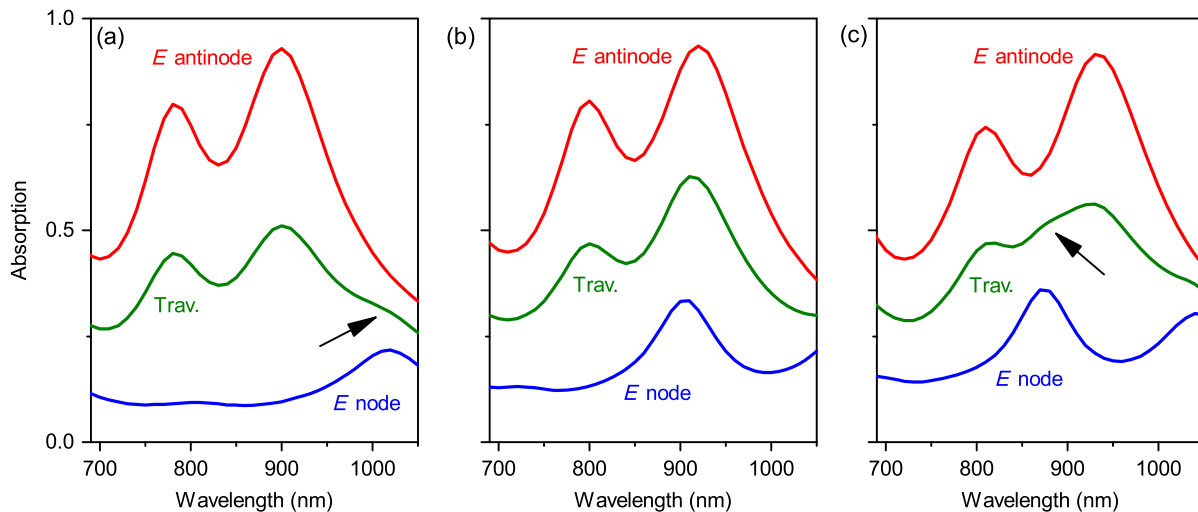


FIG. 5. Interrogating complex traveling-wave spectra using coherent spectroscopy. Numerically simulated absorption spectra are shown for three split ring slit metamaterials of different dimensions. The planar nanostructure dimensions are the same as in Fig. 4. The thickness of the middle  $\text{Si}_3\text{N}_4$  layer is (a) 30 nm, (b) 50 nm (the same sample as in Fig. 4), and (c) 60 nm. As different multipole resonances have a different dependence on the metamolecule size, the hidden resonance in (b) moves away from the Fano resonance and therefore can be seen in the traveling-wave spectra in both (a) and (c) (highlighted by arrows).

resonance comes from multipole resonances different from that of the Fano-type resonance: This peak is *different* from the peak observed at a similar wavelength in the traveling-wave excitation. This hidden resonance cannot be isolated using a conventional spectrometer (see Fig. S1 in the Supplemental Material [17] also for reflection and transmission). The very small feature at 780 nm observed in the experiment [see Fig. 4(c)] is attributed to experimental imperfections.

The multipole radiation power of the metamaterial is numerically calculated for analyzing the resonance properties and the strength of induced multipoles under different excitation conditions [38]. The electric dipole, magnetic dipole, electric quadrupole, magnetic quadrupole, and toroidal dipole are calculated. The leading terms at the  $E$  antinode and  $E$  node are shown in Figs. 4(e) and 4(f), respectively. The excitation of the sample is obviously dominated by the electric dipole resonance at the  $E$  antinode. On the contrary, magnetic dipole and electric quadrupole resonances are most strongly induced at the  $E$  node. Because the magnetic dipole and the electric quadrupole are weaker than the electric dipole by around one order of magnitude, the resonance feature at around 910 nm can easily be covered by the electric dipole resonance in the traveling-wave spectroscopy. The experimental results of Fig. 4 clearly demonstrate the capability of recovering hidden resonances of the coherent spectroscopy.

An interesting additional function of the coherent spectroscopy can be seen in Figs. 4(g) and 4(h), which show the electric field distribution at the middle plane of the metamolecule at the  $E$  antinode and  $E$  node. Near-field hot spots can be clearly seen in both cases, and their locations change with the excitation condition. They are localized inside

the straight slit at the  $E$  antinode, but appear between adjacent metamolecules at the  $E$  node. This indicates the possibility of using the coherent excitation to spatially manipulate near-field optical hot spots, a function that usually requires modulating the spatial profile of excitation light [39,40].

The coherent spectroscopy not only can recover hidden resonances from a traveling-wave spectrum as shown in Figs. 4(c) and 4(d), but also can be used to interrogate traveling-wave spectra with complex features. Figure 5 compares the simulated absorption spectra of three samples at the three different excitation conditions. One sample [see Fig. 5(b)] has been reported in Fig. 4, and the other two samples [see Figs. 5(a) and 5(c)] are different from it only in the thickness of the middle  $\text{Si}_3\text{N}_4$  layer. The traveling-wave spectra in both Figs. 5(a) and 5(c) show small plateaus which can be very difficult to interpret using conventional methods. By separating the resonances on the traveling-wave spectra using the coherent spectroscopy, we can see that the plateaus come from the magnetic dipole and electric quadrupole resonances.

## V. CONCLUSIONS

Ultrathin metamaterial films specifically designed to show complex multipole resonances give an excellent experimental demonstration of the selectivity of the coherent spectroscopy. Coherent absorption spectra measured at the field node and antinode of an optical standing wave show both an improved excitation efficiency and contrast between multipoles. These functions originate from the doubled local field intensity at the field antinode and the spatial separation of electric and magnetic fields. In principle, this technique works at arbitrarily low laser power, and can be extended to any designated wavelength regime.

This method can be useful for the characterization of subwavelength thin films of a different nature, including both metamaterials and natural materials. Although the standing wave technique is two times more sensitive than conventional traveling-wave absorption measurement, it can realistically work only with noticeable absorption at present. However, the sample position in a standing wave can be modulated at high frequency and the corresponding change in absorption can be detected by phase-locking techniques, which could greatly improve detection sensitivity. Such an opportunity does not exist in conventional traveling-wave measurement.

The technique is not only suitable for free-standing thin films, but also can be satisfactorily used for thin films on low-refractive-index substrates if (1) the substrates are antireflection coated on the side opposite to the analyte layer or (2) the films are sandwiched between two identical substrates. We also envisage that some of the analyte layers can be deliberately manufactured on very thin substrates to make them compatible with the new coherent spectroscopy. Indeed, media such as graphene and pellicle films are routinely used as thin substrates.

As progress in materials science, physics, and biochemistry is underpinned by and crucially depends on the development of analytical techniques, this coherent spectroscopy offers a simple, efficient, and uniquely informative technique with great application potential. The proposed standing-wave approach can be extended to the development of ultrafast transient spectroscopies, nonlinear spectroscopies, and polarization spectroscopies.

The data from this paper can be obtained from the University of Southampton ePrints research repository [41].

## ACKNOWLEDGMENTS

We thank Vassili Savinov, Jun-Yu Ou, Kevin F. MacDonald, Eric Plum, Pin Chieh Wu, and Yao-Wei Huang for helpful discussions. This work was supported by the Engineering and Physical Sciences Research Council of the United Kingdom (Grant No. EP/G060363/1), the Ministry of Education of Singapore (MOE2011-T3-1-005), the Ministry of Science and Technology of Taiwan (104-2745-M-002-003-ASP), and Academia Sinica of Taiwan (AS-103-TP-A06).

- 
- [1] M. L. Andersen, S. Stobbe, A. S. Sørensen, and P. Lodahl, Strongly modified plasmon-matter interaction with mesoscopic quantum emitters, *Nat. Phys.* **7**, 215 (2011).
  - [2] T. H. Taminiou, S. Karaveli, N. F. van Hulst, and R. Zia, Quantifying the magnetic nature of light emission, *Nat. Commun.* **3**, 979 (2012).
  - [3] N. Noginova, Y. Barnakov, H. Li, and M. A. Noginov, Effect of metallic surface on electric and magnetic dipole emission

- transitions in  $\text{Eu}^{3+}$  doped polymeric film, *Opt. Express* **17**, 10767 (2009).
- [4] P. K. Jain, D. Ghosh, R. Baer, E. Rabani, and A. Paul Alivisatos, Near-field manipulation of spectroscopic selection rules on the nanoscale, *Proc. Natl. Acad. Sci. U.S.A.* **109**, 8016 (2012).
- [5] S. M. Hein and H. Giessen, Tailoring Magnetic Dipole Emission with Plasmonic Split-Ring Resonators, *Phys. Rev. Lett.* **111**, 026803 (2013).
- [6] B. Rolly, B. Bebey, S. Bidault, B. Stout, and N. Bonod, Promoting magnetic dipolar transition in trivalent lanthanide ions with lossless Mie resonances, *Phys. Rev. B* **85**, 245432 (2012).
- [7] R. Filter, S. Mühlig, T. Eichelkraut, C. Rockstuhl, and F. Lederer, Controlling the dynamics of quantum mechanical systems sustaining dipole-forbidden transitions via optical nanoantennas, *Phys. Rev. B* **86**, 035404 (2012).
- [8] W. Lukosz and R. E. Kunz, Light emission by magnetic and electric dipoles close to a plane interface. I. Total radiated power, *J. Opt. Soc. Am.* **67**, 1607 (1977).
- [9] W. Lukosz and R. E. Kunz, Light emission by magnetic and electric dipoles close to a plane interface. II. Radiation patterns of perpendicular oriented dipoles, *J. Opt. Soc. Am.* **67**, 1615 (1977).
- [10] W. Lukosz, Light emission by magnetic and electric dipoles close to a plane dielectric interface. III. Radiation patterns of dipoles with arbitrary orientation, *J. Opt. Soc. Am.* **69**, 1495 (1979).
- [11] N. Noginova, G. Zhu, M. Mavy, and M. A. Noginov, Magnetic dipole based systems for probing optical magnetism, *J. Appl. Phys.* **103**, 07E901 (2008).
- [12] N. Noginova, R. Hussain, M. A. Noginov, J. Vella, and A. Urbas, Modification of electric and magnetic dipole emission in anisotropic plasmonic systems, *Opt. Express* **21**, 23087 (2013).
- [13] S. Karaveli and R. Zia, Spectral Tuning by Selective Enhancement of Electric and Magnetic Dipole Emission, *Phys. Rev. Lett.* **106**, 193004 (2011).
- [14] S. Karaveli, A. J. Weinstein, and R. Zia, Direct modulation of lanthanide emission at sub-lifetime scales, *Nano Lett.* **13**, 2264 (2013).
- [15] J. Zhang, K. F. MacDonald, and N. I. Zheludev, Controlling light-with-light without nonlinearity, *Light Sci. Appl.* **1**, e18 (2012).
- [16] X. Fang, M. L. Tseng, J. Y. Ou, K. F. MacDonald, D. P. Tsai, and N. I. Nikolay, Ultrafast all-optical switching via coherent modulation of metamaterial absorption, *Appl. Phys. Lett.* **104**, 141102 (2014).
- [17] See Supplemental Material at <http://link.aps.org/supplemental/10.1103/PhysRevApplied.5.014010> for additional details on the experiment and simulation methods, the traveling-wave spectra, and the measured and simulated coherent absorption.
- [18] Y. P. Svirko and N. I. Zheludev, *Polarization of Light in Nonlinear Optics* (Wiley, Chichester, 1998), p. 182.
- [19] N. Yang and A. E. Cohen, Local geometry of electromagnetic fields and its role in molecular multipole transitions, *J. Phys. Chem. B* **115**, 5304 (2011).

- [20] J. Brian Leen, P. Hansen, Y. T. Cheng, and L. Hesselink, Improved focused ion beam fabrication of near-field apertures using a silicon nitride membrane, *Opt. Lett.* **33**, 2827 (2008).
- [21] B. Sepúlveda, Y. Alaverdyan, J. Alegret, M. Käll, and P. Johansson, Shape effects in the localized surface plasmon resonance of single nanoholes in thin metal films, *Opt. Express* **16**, 5609 (2008).
- [22] T. Rindzevicius, Y. Alaverdyan, B. Sepulveda, T. Pakizeh, M. Käll, R. Hillenbrand, J. Aizpurua, and F. Javier García de Abajo, Nanohole plasmons in optically thin gold films, *J. Phys. Chem. C* **111**, 1207 (2007).
- [23] F. J. García-Vidal, L. Martín-Moreno, E. Moreno, L. K. S. Kumar, and R. Gordon, Transmission of light through a single rectangular hole in a real metal, *Phys. Rev. B* **74**, 153411 (2006).
- [24] Y. Alaverdyan, B. Sepúlveda, L. Eurenus, E. Olsson, and M. Käll, Optical antennas based on coupled nanoholes in thin metal films, *Nat. Phys.* **3**, 884 (2007).
- [25] F. Monticone, N. M. Estakhri, and A. Alù, Full Control of Nanoscale Optical Transmission with a Composite Metascreen, *Phys. Rev. Lett.* **110**, 203903 (2013).
- [26] C. Pfeiffer and A. Grbic, Metamaterial Huygens' Surfaces: Tailoring Wave Fronts with Reflectionless Sheets, *Phys. Rev. Lett.* **110**, 197401 (2013).
- [27] E. D. Palik, *Handbook of Optical Constants of Solids* (Academic Press, Boston, 1985), p. 899.
- [28] Z. Yin and F. W. Smith, Optical dielectric function and infrared absorption of hydrogenated amorphous silicon nitride films: Experimental results and effective-medium-approximation analysis, *Phys. Rev. B* **42**, 3666 (1990).
- [29] Z. Liu, A. Boltasseva, R. H. Pedersen, R. Bakker, A. V. Kildishev, V. P. Drachev, and V. M. Shalaev, Plasmonic nanoantenna arrays for the visible, *Metamaterials* **2**, 45 (2008).
- [30] W. Cai, U. K. Chettiar, H. K. Yuan, V. C. de Silva, A. V. Kildishev, V. P. Drachev, and V. M. Shalaev, Metamagnetics with rainbow colors, *Opt. Express* **15**, 3333 (2007).
- [31] U. K. Chettiar, S. Xiao, A. V. Kildishev, W. Cai, H. K. Yuan, V. P. Drachev, and V. M. Shalaev, Optical metamagnetism and negative-index metamaterials, *MRS Bull.* **33**, 921 (2008).
- [32] N. Liu, L. Fu, S. Kaiser, H. Schweizer, and H. Giessen, Plasmonic building blocks for magnetic molecules in three-dimensional optical metamaterials, *Adv. Mater.* **20**, 3859 (2008).
- [33] P. Grahm, A. Shevchenko, and M. Kaivola, Electric dipole-free interaction of visible light with pairs of sub-wavelength-size silver particles, *Phys. Rev. B* **86**, 035419 (2012).
- [34] J. Valentine, S. Zhang, T. Zentgraf, E. Ulin-Avila, D. A. Genov, G. Bartal, and X. Zhang, Three-dimensional optical metamaterial with a negative refractive index, *Nature (London)* **455**, 376 (2008).
- [35] B. Luk'yanchuk, N. I. Zheludev, S. A. Maier, N. J. Halas, P. Nordlander, H. Giessen, and C. T. Chong, The Fano resonance in plasmonic nanostructures and metamaterials, *Nat. Mater.* **9**, 707 (2010).
- [36] V. A. Fedotov, N. Papasimakis, E. Plum, A. Bitzer, M. Walthers, P. Kuo, D. P. Tsai, and N. I. Zheludev, Spectral Collapse in Ensembles of Metamolecules, *Phys. Rev. Lett.* **104**, 223901 (2010).
- [37] N. Papasimakis, Z. Luo, Z. X. Shen, F. D. Angelis, E. D. Fabrizio, A. E. Nikolaenko, and N. I. Zheludev, Graphene in a photonic metamaterial, *Opt. Express* **18**, 8353 (2010).
- [38] V. Savinov, V. A. Fedotov, and N. I. Zheludev, Toroidal dipolar excitation and macroscopic electromagnetic properties of metamaterials, *Phys. Rev. B* **89**, 205112 (2014).
- [39] T. S. Kao, S. D. Jenkins, J. Ruostekoski, and N. I. Zheludev, Coherent Control of Nanoscale Light Localization in Metamaterial: Creating and Positioning Isolated Subwavelength Energy Hot Spots, *Phys. Rev. Lett.* **106**, 085501 (2011).
- [40] B. Gjonaj, J. Aulbach, P. M. Johnson, A. P. Mosk, L. Kuipers, and A. Lagendijk, Active spatial control of plasmonic fields, *Nat. Photonics* **5**, 360 (2011).
- [41] DOI: 10.5258/SOTON/384842.